

Dynamic Modeling of a Cable Suspended Parallel Robot

Le Duc Duy and Nguyen Truong Think

Department of Mechatronics, Ho Chi Minh City University of Technology and Education

Thu Duc City, Ho Chi Minh City, Vietnam

Email: duyleduc123@gmail.com, thinknt@hcmute.edu.vn

Abstract—Recently, Cable Suspended Parallel Robots (CSPRs) have provided considerable advances while driving in specific fields where dynamic features are required. Representative examples include moving a large cargo in fast transitions while maintaining high precision. As a result, in order to effectively handle CSPRs on complex movements with varying payloads, dynamic restrictions must be required. By real-time measuring the force applied to each cable, we can approach the payload at any point, as the manipulators act instantly when carrying distinct objects. The inverse dynamic equation is come up using the Lagrangian formulation, and the rope mass is negligible. In order to real time measurement cable tensions, a proportional-derivative(PD) model drives each motor. Finally, simulation and experiment are used to test the stability of dynamic modeling for control and to confirm the program.

Keywords—CSPR, cable robot, PD control, dynamics, kinematics

I. INTRODUCTION

Robots have been used in a wide range of industries in recent decades. Many aspects of manufacturing and engineering, on the other hand, do not rely on robots, owing to the limitations of conventional robots [1]. For example, in many applications, workspace requirements and load carrying capacity are far greater than what conventional robots can provide, even when the robot's cost is taken into account [2]. A new class of parallel robots was introduced to solve the latter issue [3]. Cable-Suspended Parallel Robots (CSPR) are structurally similar to parallel actuated robots, with the exception that the End-Effector (EE) can only be pulled, not pushed, by the cables. Fig. 1 depicts a schematic representation of a CSPR in a general configuration. It is made up of a motor, a winch system, and an EE. Because of the behavior of the cables, feedback control of CSPR is much more difficult than that of parallel-actuated robots.

As compared with other types, CSPRs have a large workspace, a large payload, a high movement speed, easy maintenance, and are inexpensive. Those values enable them to offer many solutions not only in industrial applications, but also in a wide range of other fields. As a result, they may be utilized for 3D printing of massive structures [4] with a big footprint of 15 x 11m and 6m high, as well as surface finishing, such as painting and

sandblasting [5], to enhance the efficiency of these operations and free human operators from unpleasant tasks. Furthermore, high speed pick-and-place, up to 2,5 m/s velocity and 12 m/s² acceleration in [6]. As multi-science platform, CSPR can be a support for five-hundred-meter Aperture Spherical radio Telescope (FAST)[7], the most sensitive radio telescope, which will allow astronomers to jumpstart numerous science goals, such as neutral hydrogen line scanning in distant galaxies out to extremely large redshifts, searching for the first bright star, finding thousands of new pulsars, and so on. It should be noted that redundant actuated CSPRs are preferable to cranes for accurate pick-and-place operations and large and heavy parts since they suffer from less load swinging. Furthermore, unlike regular cranes, CSPRs can control both the position and orientation of the object. As a result, the purpose of this article is to determine a control solution for a suspended semi-industrial CSPR prototype for metal box pick and place operations. Because of the variability of the load, robust control is essential to achieve high precision and repeatability of the MP pose.

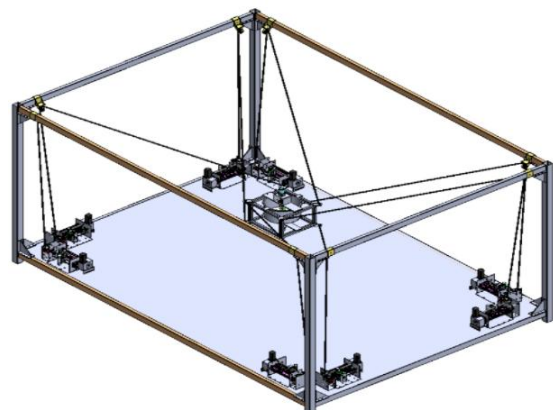


Figure 1. CSPR 3D model in suspended configuration

Several efforts have been made to model and handle CSPR in real-time [8], [9]. All kinetostatic models proposed for CSPR should have static balancing between external forces and cable tension [10]. Most popular control techniques used for conventional robots might be applied for CSPRs with the premise of no mass and no elongation for cables. PD controller is considered for almost applications that do not require strictly special working conditions. But the examples above are usually

high load and slow moving or vice versa because of the effect of dynamic features is ignored. Therefore, this paper presents control solution that real-time mass compensating feed-forward assemblies with the dynamic processing block.

The paper is organized as follows. Section 2 presents the kinematic and dynamic modeling theory in general which purposed to experiments. Section 3 mention about the control scheme and controllers. Section 4 presents an analysis of the experiment. Finally, conclusions are drawn and we present future work in Section 5.

II. SYSTEM KINEMATIC AND DYNAMIC MODEL

This section provides kinematic and dynamic model in general configuration. The prototype has 8 cables to over constrain control both the platform position and orientation. The parameters 5 m, 3 m, 3 m are length, width and height of the structure, respectively. The cables are coiled on 100mm diameter motorized winches and 8 passive pulleys guide the cable from the winches to the cable exit point. A gearbox of reduction between each motor and each winch is assembled, which have ratio equal to 30. The moving-platform (MP) of size 0.5 m×0.5 m×0.5 m and mass 153 kg.

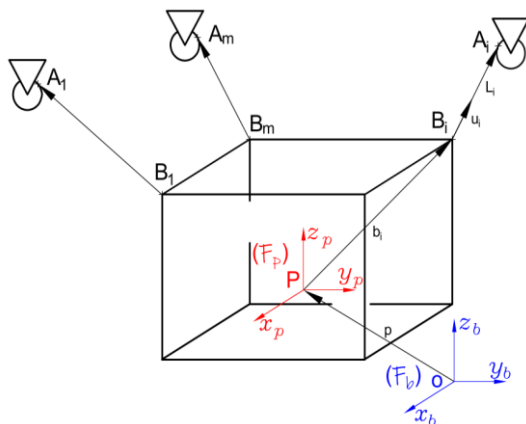


Figure 2. CSPR geometric parameters.

The inverse kinematics problem can be described as follows: Given a desired position and orientation of the payload (p, R), find the positions of the motor ($q_i, i = 1, 2, \dots, n$) that satisfy the static equilibrium and geometry constraints. To define its position in 3-D space, the platform requires three coordinates. As a result, each joint has three unknowns. Furthermore, each cable has an unknown tension. As a result, in the case of 8 cables, the total number of unknowns is 32. At least three attachment points are required for the payload to maintain its desired position and orientation. As a result, the inverse kinematics problem is unsolvable in the cases of one and two robots. There are an infinite number of solutions for cases with three or more robots, because the number of unknowns is greater than the sum of the number of static equilibrium equations and the number of constraints.

Fig. 1 illustrates schematically $n = 6$ d.o.f CSPR. A_i denotes each cable exit point at the pulley attach to base frame, while B_i expresses the attachment point to the

mobile platform. The positions of the cable attachment vector b_i points from point P to point B_i and is expressed in frame F_p . The position vector are denoted b_{pi} point from point O to point P and is expressed in frame F_b , P being the center of mass of mobile platform. Note that F_b is the global coordinate and F_p is the attached coordinates on the MP.

As with other parallel mechanisms, the inverse kinematics of a cable-suspended system is relatively simple. The vector ${}^b l_i$ of i th cable is define as follow[11]:

$${}^b L_i = l_i u_i = {}^b a_i - {}^b p - {}^b Q_p {}^p b_i \quad (1)$$

With l_i is lenght of i th cable and u_i is the unit vector of the i th cable vector, defined as:

$$l_i = \| {}^b L_i \|^2 \quad (2)$$

$${}^b u_i = \frac{{}^b L_i}{\| {}^b L_i \|^2} \quad (3)$$

${}^b Q_p$ is the rotation matrix from frame F_b to frame F_p .

$$Q = \begin{bmatrix} c_\alpha c_\beta & c_\alpha s_\beta s_\gamma - s_\alpha c_\gamma & c_\alpha s_\beta c_\gamma + s_\alpha s_\gamma \\ s_\alpha c_\beta & s_\alpha s_\beta s_\gamma - c_\alpha c_\gamma & s_\alpha s_\beta c_\gamma + c_\alpha s_\gamma \\ -s_\beta & c_\beta s_\gamma & c_\beta c_\gamma \end{bmatrix} \quad (4)$$

In Eq. (4), c stands for $\cos(\cdot)$ and s indicates $\sin(\cdot)$. Also α, β and γ are angle of rotation around z, y and x axis respectively.

By taking the first derivative of Eq. (1), $\dot{a}_i = 0$ and ${}^p b_i = {}^b \omega_p \times {}^p b_i$ the following equation is obtained[12]:

$${}^b \dot{l}_i = -u_i^T {}^b \dot{p} + ({}^p b_i \times u_i^T)^b \dot{\omega}_p \quad (5)$$

Note that ω_i is the rotational velocity of MP expressed in the F_b . Therefore the kinematic equation for the robot has the following form:

$$\dot{l} = J \dot{x} = \frac{\rho}{D} \dot{q} \quad \text{with} \quad \dot{x} = [{}^b \dot{p} \quad {}^b \dot{\omega}]^T \quad (6)$$

With ρ denote winch radius and D denote gear reducer. The x' vector include the linear and rotation velocity of MP expressed in F_b and J is the forward jacobian matrix.

$$J = \begin{bmatrix} -u_1 & {}^b Q_p ({}^b b_1 \times u_1) \\ -u_2 & {}^b Q_p ({}^b b_2 \times u_2) \\ \vdots & \vdots \\ -u_m & {}^b Q_p ({}^b b_m \times u_m) \end{bmatrix} \quad (7)$$

From [13], the dynamic model of the CSPR are written as.

$$H \ddot{x} + C \dot{x} = J^T \tau + w_g + w_e \quad (8)$$

Where: H stand for the spatial inertia matrix of the moving platform and C the matrix of the centrifugal and Coriolis wrenches.

$$H = \begin{bmatrix} m_p I_{3 \times 3} & -M\hat{X}_p \\ M\hat{X}_p & I_p \end{bmatrix} \quad (9)$$

Where: m_p presents mass of the platform. $I_{3 \times 3}$ is identity matrix. $M\hat{X}_p = {}^b Q_p [m_p x_g, m_p y_g, m_p z_g]^T$ is the first momentum expressed in frame F_b and $M\hat{X}_p$ is the skew-matrix associated to $M\hat{X}_p$. H stands for tension inertia matrix. We can obtain the platform's inertia tensor I_t using Huygens-Steiner's theorem, then compute H .

$$H = {}^b Q_p I_t {}^b Q_p^T - \frac{M\hat{X}_p M\hat{X}_p}{m_p} \quad (10)$$

$$\text{With } I_t = \begin{bmatrix} I_{xx} & I_{xy} & I_{xz} \\ I_{yx} & I_{yy} & I_{yz} \\ I_{zx} & I_{zy} & I_{zz} \end{bmatrix} \quad (11)$$

During platform movement, centrifugal and Coriolis forces have an impact on it and define the following:

$$C\dot{x} = \begin{bmatrix} {}^b \hat{\omega}^b \hat{\omega} M\hat{X}_p \\ {}^b \hat{\omega} I_t^b \omega \end{bmatrix} \quad (12)$$

As the C.O.M of the moving platform does not coincide, the wrench caused by gravity is defined as:

$$w_g = \begin{bmatrix} m_p I_{3 \times 3} \\ M\hat{X}_p \end{bmatrix} \quad (13)$$

III. CONTROLLER SOLUTION

We present a basic control method using PD controllers in this section. In the next step, we add a feed-forward term to the controller that anticipates for the MP dynamics and compensates for a mass along the trajectory. The following control schemes treat all signals as vectors because of the parallel nature of CSPRs. Motor position and velocity are inputs to every actuation chain, from motor to cable. Output is the torque desired by the motor. The eight decentralized controllers here have been adjusted similarly. To compensate for the losses in transmissions, it implement a linear friction model in each actuation chain[10].

$$\tau_{MO} = F_s \text{sign}(\dot{i}) + \frac{F_v D}{\rho} \dot{i} \quad (13)$$

Where: i being marked cable velocity vector and τ_{MO} being the generated friction compensation. The viscous friction coefficients for each motor are represented by the F_v, I_{MO} means moment of inertia. The initial element of the control scheme used on this robot is based on a well-known proportional-derivative strategy in robotics. Fig. 3 shows the control scheme, which includes the intended Cartesian location and orientation of the MP as 6-

dimensional vector x , the desired MP twist x' , the 8-dimensional vector of wanted motor angular positions q_{de} , and the 8-dimensional vector of desired motor torques τ . K_p and K_d are the controller's proportional and derivative gains, adjusted so that the robot can attain precision and stability using only the MP. In the two additional controllers, the identical settings were utilized. It is feasible to add a term to the controller based on the robot's dynamic model that anticipates MP dynamics and compensates for a particular mass along the trajectory.

$$\tau_{ID} = A^+ (-H\ddot{x} - C\dot{x} + w_g + w_e) \frac{d_\omega}{D} \quad (15)$$

Where: τ_{ID} the feed-forward torque, m_p the compensating mass includes the platform and its eventual load, g the vector representing gravity in the base frame, D the winch radius, and d_ω the gearbox reduction. $A = -J^T$ denotes the wrench matrix, A^+ represents A 's Moore-Penrose pseudoinverse. This figure shows the PD control system with feedforward (PDFF), which includes x'' cartesian and angular accelerations for the platform.

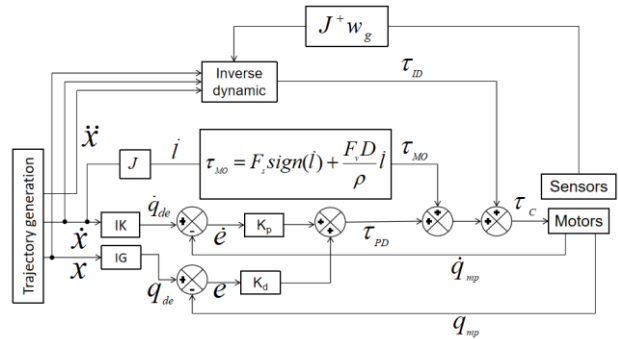


Figure 3. The PD controller with dynamic processing block feed-forward and a real-time mass compensating block.

It's worth updating the mass in the compensation term to increase robustness, especially if the items in question have a wide range of forms, sizes, and weights. With the following assumptions: The platform has a low linear and angular velocity; Due to the carrying payload, particularly the metal plate, the platform has just one wrench applied to it; The cables are stiff and unyielding.

The inertial and Coriolis effect on the platform can be neglected and Eq. (8) can be rewritten as:

$$J^T \tau = w_g \quad (16)$$

Using the wrench matrix A and the cable tension vector τ obtained by the dynamometers, it is then feasible to compute the payload mass m_p and the Cartesian coordinates x_G and y_G of the center of mass of the set formed of the moving-platform and the carried payload [9], w_g represented in Eq.(13). For the duration of the test, assume a null platform orientation. Eq.(16) becomes.

$$J^T \begin{bmatrix} \tau_1 \\ \vdots \\ \tau_i \\ \vdots \\ \tau_8 \end{bmatrix} = \begin{bmatrix} 0 \\ 0 \\ -m_p g \\ -m_p g y_g \\ m_p g x_g \\ 0 \end{bmatrix} \quad (17)$$

Thus, it able to add an input to the inverse dynamic block with compensation term of mass to feed the real-time estimation the pay load.

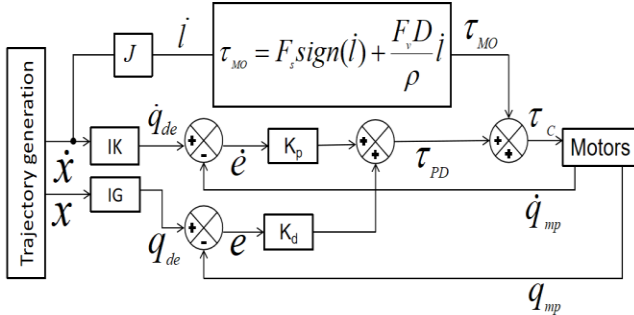


Figure 4. The PD basic controller.

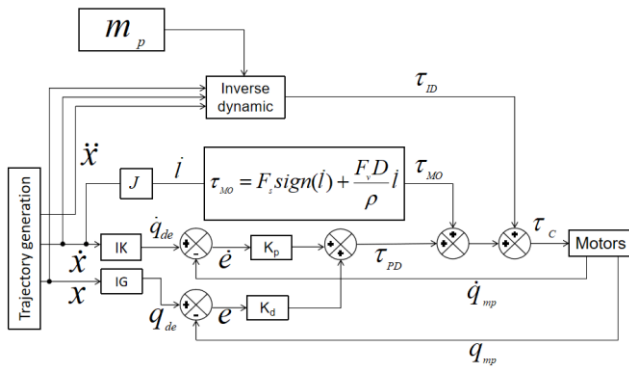


Figure 5. The PD controller with dynamic processing block feed-forward.

IV. SIMULATION STUDIES AND EXPERIMENTAL RESULTS

A. Simulation Example Studies

After the implementation of the algorithm, simulations are conducted in order to compare the dynamic model with the static model. From there, draw conclusions about the influence of dynamic parameters on the accuracy and stability of the robot. The simulation has the following main characteristics:

- + The cable configuration shown in Fig. 6, $m = 8$ cables so that the prototype has 2 degrees of actuation redundancy. This is over-constrain structure so that the moving platform can be handle flexibly on both position and orientation.
- + 8 100mm diameter winches which be actuated by 8 motors.
- + The dimensions of the base frame are 5x3x3 m.
- + The overall dimensions of the plat form are 26.5x23.5x22 cm, and it weighs 153 kg.
- + The payload weights 200 kilograms. As a result, the total mass of the moving object is 353 kg.

+ The platform's reference frame is placed in the ideal center of mass.

The simulation is carried out by defining the desired trajectories and velocity functions ahead of time. The sample time is 0.1 second. In the second step, tensions are calculated and compared between the two models. The tension applied to the 8 cables of the two models is then calculated and compared. Gradually increase the moving speed, change orientation and mass to draw results on the influence of dynamic parameters.

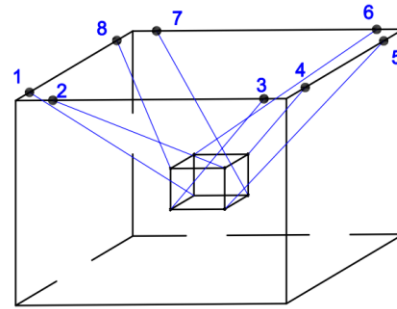


Figure 6. CSPR configuration.

First, we produce motion trajectories on the x,y,z axes without changing the orientation, and a travel speed is derived from its motion equation. First, we create motion trajectories on x,y,z axes without change in orientation and travel speed corresponding to 20s simulation. The trajectories are divided into two parts. The difference in the two parts is that the first has a second order equation that can be derived twice, resulting in constant acceleration, whereas the others do not. The goal is to investigate the effect of the inertia wrench on tension deviation when two models are compared. The moving platform's mass remains constant, and the cable elasticity is negligible. The motion is shown in Fig. 7 and the equations of trajectory is shown below:

$$x = \begin{cases} 20(5-t)^2 & 0 \leq t \leq 10 \\ 500 - 10(t-10) & 10 < t \leq 20 \end{cases} \quad (18)$$

$$y = \begin{cases} 60(5-t) & 0 \leq t \leq 10 \\ -300 + 20(t-10) & 10 < t \leq 20 \end{cases}$$

$$z = \begin{cases} 20t & 0 \leq t \leq 10 \\ 200 - 10(t-10) & 10 < t \leq 20 \end{cases}$$

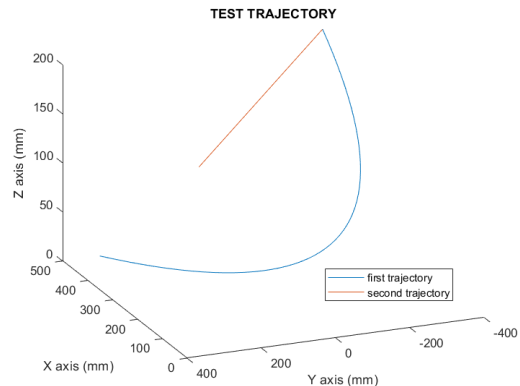


Figure 7. Test trajectory.

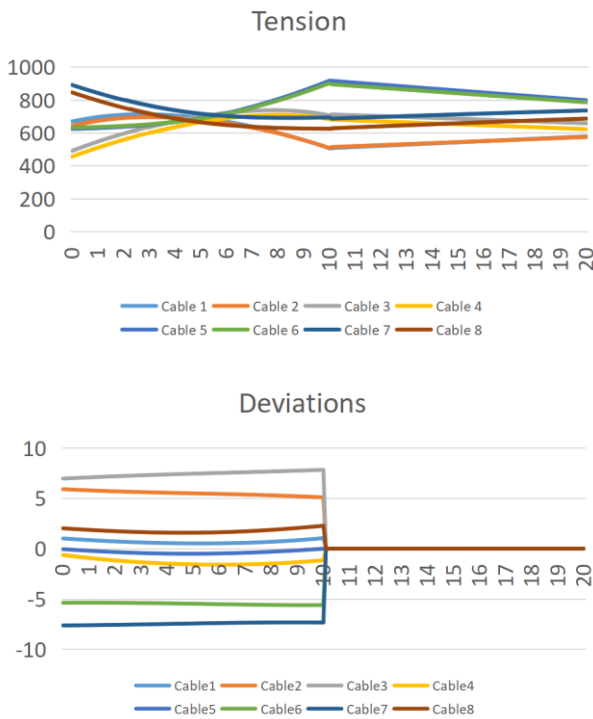


Figure 8. The tensile forces diagram of dynamic model controller and the deviation when compared to the static model controller.

Fig. 8 depicts the tension diagrams of the simulation and the deviations when compare two models during motion. It is clear that the inaccuracy is greater in the time interval 0 to 10 s when the motion has the acceleration in x axis. When the acceleration variable is lost, the errors immediately reduces to zero. This demonstrates that the inertial wrench has a significant impact on precision. The effects of the Coriolis effect and centrifugal force on the moving platform are then investigated in a second experiment. Allow the platform to move the same distance but in half the time in the next simulation. Then we modify the direction of the x and y axes by 5 degrees respectively. The following motion functions are represented:

$$\begin{aligned}
 x &= \begin{cases} 80(2.5-t)^2 & 0 \leq t \leq 5 \\ 500 - 20(t-5) & 5 < t \leq 10 \end{cases} \\
 y &= \begin{cases} 120(2.5-t) & 0 \leq t \leq 5 \\ -300 + 40(t-5) & 5 < t \leq 10 \end{cases} \\
 z &= \begin{cases} 40t & 0 \leq t \leq 5 \\ 200 - 20(t-5) & 5 < t \leq 10 \end{cases}
 \end{aligned} \tag{19}$$

We receive the following results after running the simulation. We collect variables such as the highest value, median value, and RMS value of tension variation for each cable in both the first and second simulations to better understand the effects of speed on precision.

The results demonstrate that the parameters collected differ significantly between the two simulations. This is especially noticeable in cables 2, 3, 6, and 7, where the

RMS and median values are clearly different. They explain why characteristics like inertial force, Coriolis effect, and speed of rotation operate on the moving platform, causing increasing tension on each cable, after running two simulations. In the third simulation, we suppose that the mass changes. The trajectory programs remain unchanged from the second simulation. At the third second, add 100 kg to the load. This simulation only executed the first orbital move to demonstrate the impact. The results based on the first cable's parameters are displayed in Fig. 9.

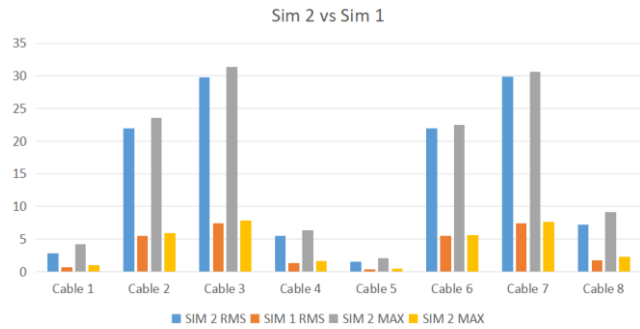


Figure 9. Max, median and RMS values of deviation of each tensile force in each model controller.

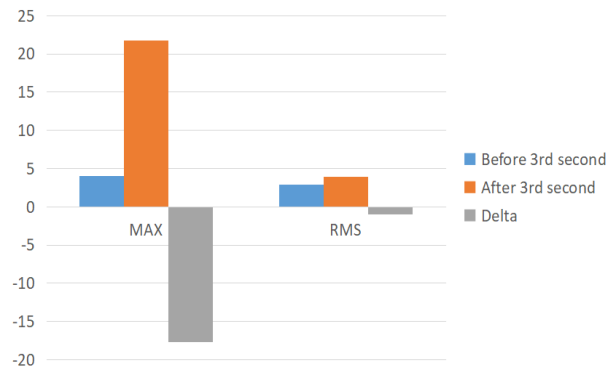


Figure 10. The errors when compares in two interval time, before and after 3rd second, of the first cable.

According to the graph, after raising the weight by 100 kg at time $t=3s$, all delta parameters had negative values, indicating a greatly increased deviation. The dynamic model demonstrates its efficiency when high-speed platform motions, complex motion patterns, movement orientations, and massive weights are required. When the variables of velocity, orientation, and mass are changed in the above three simulations, there is an obvious rise in errors. The static model solely examines gravity, whereas the dynamic model takes into account gravity, inertia, Coriolis, and centrifugal force. As a result, the fundamental reasons for the distinction between dynamic and static models include features such as shape, velocity, and acceleration. It is critical to correctly determine the center of mass in order to decrease computational work. That is one of the most common sources of errors in experiments, and it is straightforward to predict.

B. Experimental Results

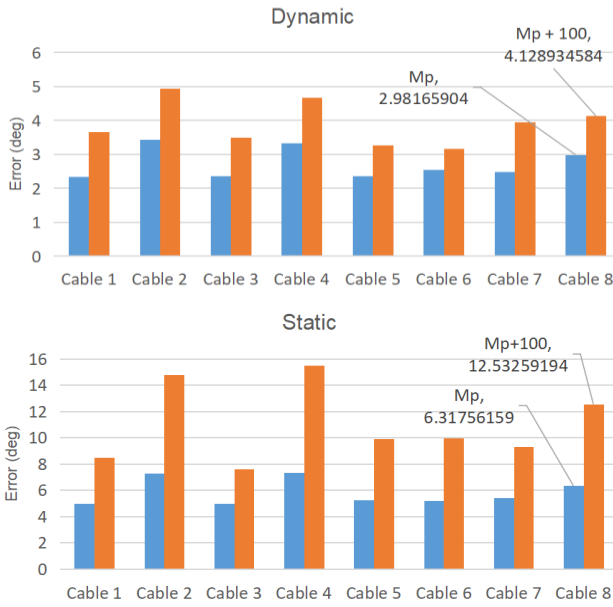


Figure 11. Root Mean Square (RMS) of position error(degrees) for Motors 1 to 8 (left to right) against load.

We compare the actual tension on the cables with simulations in this experiment. Sensors will be installed to determine the value of tension applied to the cables. On the other hand, because we have no equipment to precisely measure the position of the platform, we will calculate errors based on the position and speed of the motor shaft. Check the real-time mass compensator and the dynamic parameter processing block for efficiency as well.

The experiment use the same parameters as the previous simulation but the sample time down to 0.5 second. Then gather the results of the tension during the movement and compare them to the simulation results. Observe the position and velocity errors on each motor, on the other hand, to estimate the platform's position and velocity errors. Third, gather the real-time mass compensator's data and compare it to the actual mass. Fig. 9 presents the Root Mean Square (RMS) of Motors 1 to 8 position errors along the trajectory for each model. As expected, the errors are generated by static model control is high, up to 15 degrees. The errors increase when mass added to the payload as the result obtained form simulations. Clearly differences in the performances from the dynamic model to the static model could be explained by the real-time mass compensator is working well. In the next step, a single motor is considered to observe its error along trajectory for each model and load. Fig. x presents angular errors of the 3rd motor when running this test. Again, the error during test trajectory of static model is higher. Call delta as a difference between two model controllers, it seem to be clear that delta has positive values for almost time. On the other hand, at starting time and the transition time from the 1st trajectory and 2nd trajectory is rapidly increase due to the huge changes in

velocity, acceleration and orientation of the platform. These results prove that the simulation was right.

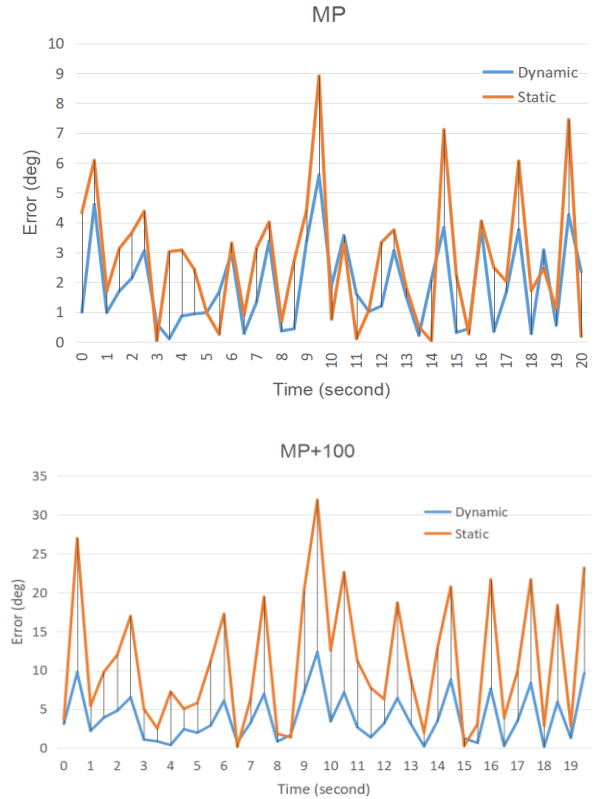


Figure 12. Motor 3rd position error eq,3 (degrees).

V. CONCLUSION

A new control strategy for cable-driven parallel robots (CSPRS) has been proposed, constructed, and tested on a test pick-and-place trajectory with various masses using a PD torque controller with a real-time mass estimation and compensation term. It has shown feasible to continually update the feedforward term to adjust for any payload using the mass estimation from the dynamometer readings, achieving equivalent performance to a PD controller with feedforward and exact knowledge of the mass. While the PD controller can be fine-tuned for each situation, the suggested controller can adapt to the payload, boosting robot accuracy. The proposed control schemes' stability will be goes on to explain. Furthermore, a sensitivity analysis will be carried out in order to establish the appropriate controller tuning parameters. Further testing will be performed to assess the method's robustness in the face of strong moving-platform accelerations. A better model of the robot could help improve mass estimate by accounting for the motion of cable exit points caused by pulleys. Finally, the robot's behavior in response to variations in payload mass during the trajectory will be investigated in the future.

ACKNOWLEDGMENT

Authors would also like to thank the Ho Chi Minh City University of Technology and Education in Vietnam for providing financial support and study facilities.

REFERENCES

- [1] P. Dewdney, M. Nahon, and B. Veidt, "The large adaptive reflector: A giant radio telescope with an aero twist," *Canadian Aeronautics and Space Journal*, vol. 48, no. 4, pp. 239-250, 2002.
- [2] S. Kawamura, "Development of an ultrahigh speed robot FALCON using wire drive system," *Robotics and Automation*, pp. 215-220, 1995.
- [3] J. Brest, S. Greiner, B. Boskovic, M. Mernik, and V. Zumer, "Self-adapting control parameters in differential evolution: A comparative study on numerical benchmark problems," *IEEE Transactions on Evolutionary Computation*, vol. 10, no. 6, pp. 646-657, 2006.
- [4] J. B. Izard, A. Dubor, P. E. Hervé E. Cabay, D. Culla, M. Rodriguez, and M. Barrado, "Large-scale 3D printing with cable-driven parallel robots," *Construction Robotics*, vol. 1, no. 1, pp. 69-76, 2017.
- [5] L. Gagliardini, S. Caro, M. Gouttefarde, P. Wenger, A. Girin, "A reconfigurable cable-driven parallel robot for sandblasting and painting of large structures," *Cable-Driven Parallel Robots*. Springer, pp. 275-291, 2015.
- [6] S. Kawamura, H. Kino, and C. Won, "High-speed manipulation by using parallel wire-driven robots," *Robotica*, vol. 18, no. 1, 2000.
- [7] R. Nan, "Five hundred meter aperture spherical radio telescope (FAST)," *Science in China Series G*, vol. 49, no. 2, pp. 129-148, 2006.
- [8] H. Guo, Y. Liu, G. Liu, and H. Li, "Cascade control of a hydraulically driven 6-DOF parallel robot manipulator based on a sliding mode," *Control Engineering Practice*, vol. 16, no. 9, pp. 1055-1068, 2008.
- [9] C. Woernle, "Dynamics and control of a cable suspension manipulator," in *Proc. 9th German-Japanese Seminar on Nonlinear Problems in Dynamical Systems-Theory and Applications*, Universit ät Duisburg, 2000.
- [10] M. Hiller, S. Fang, S. Mielczarek, R. Verhoeven, and D. Franitza, "Design, analysis and realization of tendon-based parallel manipulators," *Mechanism and Machine Theory*, vol. 40, no. 4, pp. 429-445, 2005.
- [11] E. Picard, E. Tahoumi, F. Plestan, S. Caro, and F. Claveau, "A new control scheme of cable-driven parallel robot balancing between sliding mode and linear feedback," *IFAC-PapersOnLine*, vol. 53, no. 2, pp. 9936-9943, 2020.
- [12] A. Aflakiyan, H. Bayani, and M. T. Masouleh, "Computed torque control of a cable suspended parallel robot," in *Proc. 2015 3rd RSI International Conference on Robotics and Mechatronics*, (ICROM). IEEE, 2015, October, pp. 749-754.
- [13] L. Gagliardini, M. Gouttefarde, and S. Caro, "Determination of a dynamic feasible workspace for cable-driven parallel robots," *Advances in Robot Kinematics*, pp. 361-370, Springer, Cham, 2018.
- [14] A. Pott, "Influence of pulley kinematics on cable-driven parallel robots," *Latest Advances in Robot Kinematics*, pp. 197-204, Springer, Dordrecht, 2012.

Copyright © 2022 by the authors. This is an open access article distributed under the Creative Commons Attribution License (CC BY-NC-ND 4.0), which permits use, distribution and reproduction in any medium, provided that the article is properly cited, the use is noncommercial and no modifications or adaptations are made.



Nguyen Truong Thinh is Dean of Faculty of Mechanical Engineering at Ho Chi Minh City University of Technology and Education, Vietnam. He is also Associate Professor of Mechatronics. He obtained his PhD. In 2010 in Mechanical Engineering from Chonnam National University. His work focuses on Robotics and Mechatronic system. Projects include: Service robots, Industrial Robots, Mechatronic system, AI applying to robot and machines, Agriculture smart machines...



Le Duc Duy is Mechatronics Engineer specializing in Cable Suspended Parallel Robot – is a member of OPEN laboratory at Ho Chi Minh City University of Technology and Education